Computational Fluid Dynamic Simulation of Heat Transfer in Designed Natural Convection Novel Solar Dryer

For use in the Himalayan Regions

Lhakpa Tempa Waiba

Division of Heat Transfer

Department of Energy Sciences

Faculty of Engineering | Lund University

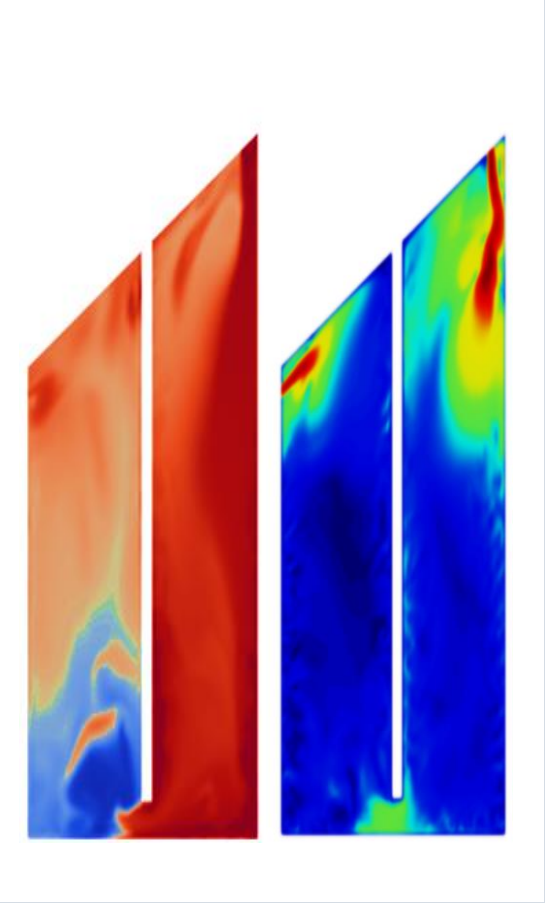

May, 2022 | Lund University

Computational Fluid Dynamic Simulation of Heat Transfer in Designed Natural Convection Novel Solar Dryer

For Use in the Himalayan Regions.

Dissertation for the Master of Engineering in Renewable Energy.

In collaboration with Lund University and College of Science and Technology

Author: Lhakpa Tempa Waiba

Royal University of Bhutan

College of Science and Technology

July, 2022

Principal Supervisor: Dr Himani Garg

Division of Heat Transfer

Faculty of Engineering

Lund University

Supervisor: Dr Tshewang Lhendrup

Jigme Namgyal Engineering College

Royal University of Bhutan

Acknowledgement

I would like to whole heartedly thank Dr Himani Garg for constantly guiding and being my exceptional supervisor and mentor. My sincere appreciation goes to Dr Martin Andersson for all the support and guidance throughout the completion of this Dissertation at Lund University. I am highly indebted to Dr Henrik Davidsson for all his support and guidance, making sure my stay at Lund is convenient and fruitful.

I would like to convey my warm gratitude to all the students at Heat Transfer Division (Lund) for sharing their in-depth experiences and taking their time to make sure that my stay at Lund University is fruitful and memorable.

I would like to thank Dr Tshewang Lhendrup and Mr Cheku Dorji for giving me this wonderful opportunity to do a solar food project as my master Dissertation and for their continued support and motivation despite their busy schedule.

I would also like to thank the Royal University of Bhutan (RUB) and Lund University for providing the necessary support and making my journey to Sweden smooth and comfortable.

Lastly but not the least, I would like to thank my family, friends and everyone involved in this journey for always believing in me without whom this dissertation wouldn't have been successful.

Preface

This master Dissertation is a part of the project Solar Food: *Reducing post-harvest losses through improved solar drying* (VR-2020 -04071). The project is a collaboration between Lund University, Kathmandu University, Royal University of Bhutan and Ruralis- Institute for Rural and Regional Research. The final goal of the project is to improve farmer's livelihood and contribute rural development by developing a locally adapted solar dryers for crop drying with short drying times. The project will span over the course of three years and is funded by the Swedish Scientific Council in collaboration with the Swedish International Development Cooperation Agency. The project is being coordinated by Dr Martin Andersson and Dr Henrik Davidsson at Lund University.

Abstract

This dissertation presents the numerical analysis of natural convection Novel solar dryer through CFD simulation by using finite volume approach to study the heat transfer dynamics and thermal performance of the airflow within the computational domain of designed natural convection solar dryer. The simulation is done for fair weather around solar noon when the collector receives maximum solar radiation and dryer is working at peak performance. The characteristics of the air flowrate (U), temperature variations (T) and air velocity profile (u) were studied inside the dryer cabinet with different values of heat transfer coefficient (h). The simulation results show that the minimum time required for maximum average temperature to reach inside the proposed solar dryer is 55.260 minutes, assuming that the maximum average temperature (T_{max}) of 82.0 ^{0}C/355K flows from the inlet. For maximum average temperature (T_{max}) of 65.0 ^{0}C, the minimum time required is 45.033 minutes. This d issertation is expected to assist in contributing additional information to the existing experiment data under the solar food project.

***Keywords*:** Computational Fluid Dynamic; Natural Convection Novel Solar Dryer; Maximum Average Temperature; Temperature Variations; Velocity Distribution; Air Flowrate.

Table of Contents

List of Figures

List of Tables

1 CHAPTER 1: Background

1.1 Introduction

Engineers and developers around the globe are using computerised technologies to model and develop prototypes rather than building a physical model to achieve the desired level of performance (Demissie,2019). This method can help investors reduce their overall project cost and avoid material waste from false testing and wrong assumptions (Roldan, 2019). Similarly, the development of solar dryers should undergo rigorous research and development (R&D) before implementing them in the field without escalating the costs associated with it.

In developing the high-performance and energy-efficient solar dryer, it is good to mathematically simulate the fluid dynamics with the help of computational tools for solving complex numerical problems. The Computational Fluid Dynamic (CFD) is the commonly used tool for the design and analysis of a system involving fluid flow, heat transfer and associated phenomena (Versteeg and Malalasekera, 2007). CFD is becoming popular in the computer-aided engineering phase for fluid dynamics studies such as temperature, velocity and pressure density (Jamshed, 2015).

There are several studies done on CFD analysis of natural convection solar dryer (NCSD) and force convection solar dryer (FCSD) using CFD tools such as ANSYS Fluent, COMSOL, SOLIDWORKS® Flow Simulation and Sim Scale and programming platforms such as C++, MATLAB, TRNSYS and Fortran (Roldan, 2019). However, there are no specific studies carried out for NCSD and FCSD using OpenFOAM CFD software. Unlike other CFD tools, Openfoam is compatible for both 2D and 3D geometry and allows users to customise their own solvers, C++ coding algorithms and numerical equations involving dynamic behaviours of fluid flow and heat transfer mechanism (Weller, et. al., 1998). Moreover, the key advantage of using Openfoam has to be its access to free license that is very helpful for those students interested in learning CFD.

1.2. Literature review

Benjamin, tested the mixed-mode solar dryer with the incorporation of an additional backup heater. In his dissertation, the performance evaluation of the solar dryer with and without a backup heater was studied. The test result found that the drying rate of the crop is dependent on the density of the crops and enhances when an additional backup heater is used.

Adelaja, et al., established a natural convection indirect type solar dryer and evaluated thermal parameters. Plantain fillets were used as a test crop for studying the efficiency and effectiveness of their system. Through their experiment, the efficiency of the collector and the system efficiency was found to be 46.4% and 78.73% respectively. The collector has a moisture removal rate of 77.5% in 20 hours of drying time.

Simate, developed a mixed-mode solar dryer for drying maize grain. The models are run under different solar conditions and then compared the result with the indirect mode natural convection solar dryer. The comparison analysis found that the collector size for a mixed-mode dryer required a shorter length for the same amount of grains than that of an indirect passive solar dryer. The author concluded that the initial cost, operation cost and maintenance cost of mixed-mode solar dryers is less than indirect passive dryers.

Weefer, did similar research on the mixed-mode passive solar dryer and studied the performance analysis by presenting the drying kinetics. In his model, tomatoes were dried under low humidity and achieved a maximum temperature of 39.2 ^{0}C inside the chamber. The author was able to dry 2 kg of tomatoes with a drying rate of 2.88 units/day. From the performance analysis result, it was found that solar irradiance, material selection, and inlet temperature greatly affect the performance of the dryer.

Ismail, designed the indirect force convection solar dryer with thermal energy storage and an in-built dehumidifier. The design consists of four major parts (solar air collector, dehumidifier, drying chamber, and thermal energy storage). PCM was a material used for thermal storage, the performance evaluation found that the drying rate inside the chamber was increased by 20% when a dehumidifier is inbuilt between the absorber plate and the glass cover of the air collectors. The dryer has a capacity of 100 kg and a maximum allowable temperature of 60 ^{0}C.

Sanghi, Ambrose & Maier., presented a paper on CFD simulation of natural convection solar dryer for corn drying process under fair and over-cast weather conditions. The performance of the solar dryer was studied and predicted certain thermodynamic parameters such as temperature, humidity and velocity profile. The simulation results were validated with the experimental results and found that temperature and humidity were 8.5% and 21.4% more than the experimental results. The paper also discusses the stagnation in the airflow from their model.

Chavan, et.al., developed a CFD model of an indirect solar dryer for drying grains to preserve during post-harvest seasons. They proposed an energy-efficient geometry for optimum performance by optimizing the sizing and placement of the fan and computing the performance through CFD simulation. The hot air from the inlet of the domain was recirculated to increase performance and efficiency. The dryer performance was determined by considering parameters such as temperature, pressure and airflow rate.

Demissie., et. al., studied an indirect mode solar dryer using CFD simulation and validated the results with the experimental results. The geometry consists of a symmetrical plane with two columns each consisting of four rack shelves. The CFD results show that the airflow is uniform at the upper shelves compared to the bottom shelve. The airflow velocity was found to be 0.14 m/sec for the lowest shelf and 0.12 m/sec for the rest of the shelves. The decrease in the airflow velocity was due to the cooling of the air as the air passes from the bottom to the top of the chamber with respect to time. From their studies, the maximum average temperature difference between the measured temperature and the CFD simulation was found to be 4.3 ^{0}C which makes their prediction qualitative and reliable.

1.3. Current Agriculture Scenario in Nepal and Bhutan

1.3.1. Bhutan

The agricultural sector in Bhutan is one of the largest revenue contributors to Bhutan besides hydropower and Tourism. Bhutan has a total territory of 38,394 square kilometres of which only 13.5% is used as of 2018 for agriculture farming. According to the labour force survey report, 2021 (National Statistics Bureau, 2021), 49.2% of the total population is employed in the agricultural sector. With enriched biodiversity and adequate monsoon rainfall, agriculture farming is cheap and requires less input. However, due to the cold and dry winter season, agricultural productions within the country become deficient and during the favourable season, it becomes excessive and a waste.

1.3.2. Nepal

Nepal has a similar geographical condition as that of Bhutan but is much larger than the former and need to look for large scale productions. Agriculture sector in Nepal provides 38% of GDP and according to Federation of Nepalese Chambers of Commerce & Industry (FNCCI, 2022), 68% of Nepal's population depends on agriculture farming. The agricultural sector in Nepal contributes 24.5% of GDP besides industries (13.7%) and service sector (61.8%). Nepal has a total area of 147,181 square kilometres of which only 21.88% is used as of 2019 for agriculture farming (The Economic Activity Report, 20/21). With huge potential still untouched in the agriculture productions, reduction of post-harvest losses in Nepal will immensely benefits the country's GDP growth.

1.4. Solar Crop Drying Technology

The traditional way of using crop drying practice is by using the sun as the main source of heating. This method however is less efficient due to various external factors such as wind, insects, fungus and micro-organisms (Tamate et al.,2017). Moreover, the price hike for fossil fuels is becoming not only expensive but also causes environmental pollution. The cost of having an electric crop dryer is not only expensive but also a post burden to the existing power grid (Nwakuba et al., 2020). To mitigate these challenges, there is a need for coming up with a suitable technology which is affordable, secure and environmentally safe.

Hence, a solar crop dryer is a renewable energy technology that uses the sun as the primary source of energy. A solar crop dryer is based on the working principle of a solar air heating system (Zomorodian, et al, 2012). A solar air heater uses the solar thermal absorber to receive

the heat energy from the sun in the form of solar radiation (isolation). The air is then passed through the absorber from the air collector to pick up heat. Solar air collectors are categorised into two, known as glazed and unglazed solar air heating systems. Glazed solar air collectors are also called transparent air collectors and are mainly used for the heating ambient temperature of industrial and commercial applications. Unglazed solar air collectors are the recirculating type used for space heating.

Solar crop drying is the technique of drying fruits and vegetables enclosed in a closed chamber by using a solar collector to absorb energy from the sun. The solar dryer consists of two-component structures, a solar air heater and the dryer cabinet. The cold air from the atmosphere is passed through the collector and heated by the absorber plate that absorbs solar radiation. The double air pass absorber and absorbers with fins are generally preferred to increase the efficiency of the solar air collector. The warm air from the collector passes through the enclosed cabinet where the stack of trays to dry crops. The moist air in the cabinet escapes into the atmosphere from the chimney.

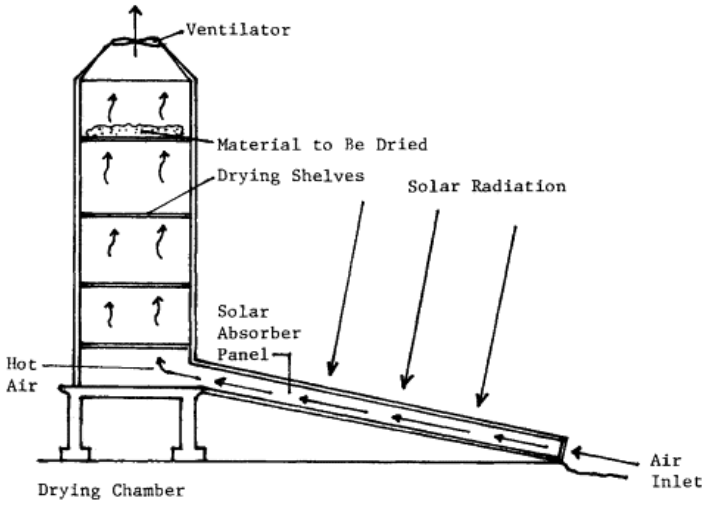

Figure 3.1: Schematic view of natural conventional solar crop dryer, Gupta, (1982)

It is different from the traditional way of drying in the open area as in this system, it does so in a controlled manner retaining the same nutrients value, colour and texture when in fresh for post-harvest consumption (Tamate et al.,2017). Solar crop drying technologies come in various geometry and size according to the needs and locations that are powered either by electricity, fossil fuel, biomass or solar energy (Olaoye et al., 2014). Solar dryers are classi-

fied into different categories direct, indirect, mixed-mode, and hybrid solar dryers. Some of the existing crop dryers are: (Nortan, 2022)

1. Mode of operation

a) Active solar dryer

The active solar dryer uses external force such as fan/ventilators to force the air into the crop drying chamber. The humidity in the closed chamber is quickly maintained within the chamber so that uniform heat is distributed inside it. This type of dryer is expensive due to extra costs incurred by the pump/fan and power supply for the operation (Ismail, 2019).

b) Passive solar dryer

A passive solar dryer is also called natural convection solar dryer. In a passive solar dryer, the air circulation in the chamber is by natural convection. In this type, the rate of moisture removal is slow compared to active solar (Hoffmann, 2021).

2. Type of solar radiation received by the absorber.

a) Indirect solar dryer

In this type of dryer, the crops are not directly exposed to the sun but solar radiation is first passed through the collector and then towards the chamber. Uniform removal of moisture from the crops is maintained in this type (Weefer, 2017).

b) Direct solar dryer

As the name suggests, the mode of operation is mainly the heat radiation passed through the sheet of transparent materials, or in some cases, the crops are directly exposed in the open area where there is the adequate sun. It is the simplest form of the solar dryer but takes longer duration for drying the crops.

c) Mixed-mode solar dryer.

The mixed-mode solar dryer is a combination of direct and indirect solar dryers. The top of the dryer is made transparent so as to transmit solar radiation. Additionally, one or more solar collectors are also attached to the dryer for indirect heating.

d) Hybrid Solar dryer

A hybrid solar dryer uses a combination of two or more heat sources such as a solar and backup heater or energy storage system (EES).

1.5. Research Motivation

i. Low post-harvest production deficits self-sufficiency in the country (Self-Sufficiency and Dietary Energy Supply of Food Crops in Bhutan, 2021)

Food security is still a big challenge for a developing nation due to poor post-harvest management and inadequate technologies. Bhutan is never an exception when it comes to post-harvest loss and management. A study survey shows an average, a Famers in Bhutan lose 180.13 Kg of Chilli annually from harvesting until it reaches packaging units (Wangmo & Dendup, 2021). A similar report on post-harvest loss for apples in the country was estimated at 12.78% of the total productions excluding the apples that are partially damaged (Rinchen, 2019).

ii. Huge investment in imports of goods during the post-harvest season (Agriculture Research and Development Highlights, 2019)

Most of the time, agricultural products go to waste due to poor post-harvest management, especially in developing countries. For example, in Bhutan, the government spends huge expenditures to import vegetables during winter.

iii. Low quality and non-nutritious value in traditional crop drying practice.

The traditional sun drying method is prone to insects, moisture and fungus. These reduce the quality and nutritious value of the crops discourages farmers and market sectors.

iv. Existing technology used in Bhutan and Nepal to dry crops is energy-intensive and inconvenient.

Most existing crop dryers are not designed and developed according to geographical locations and climatic conditions. Moreover, the performance was not optimised and as a result, this has made the existing solar dryers less efficient and energy-intensive devices.

1.6. Aim and Research Questions

This report presents the CFD study of heat transfer in designed natural convection Novel solar crop dryer under the *Solar-Food* project. The report aims to answer some of the thermodynamic parameters through CFD simulation by using the finite volume method and present answers to the some of the following research questions:

i. What is the heat transfer rate inside the designed dryer chambers in an ideal and practical working conditions?

ii. What the minimum amount of time required to reach an acceptable temperature range for drying crop?

iii. What is the overall heat lost in the designed solar dryer?

1.7. Expected Outcomes

Upon successful completion of this thesis,

i. It will provide a platform to explore software related to CFD and how to implement from the computerized system to the real world.

ii. To study the mechanisms of thermodynamics and related parameters associated with this thesis.

iii. Upcoming researchers will be able to refer the simulation results and the process concern with CFD for Novel solar dryer.

iv. To implement the developed solar dryer during post-harvest seasons from small to large scale production.

2. CHAPTER 2: Methodology

The finite volume approach is applied to study the heat transfer by natural convection inside the solar food dryer. The partial differential equations governing the energy, momentum, and mass transfer are integrated over a control volume and discretized to form sets of algebraic equations. These equations are executed in the CFD tool OpenFOAM v.7 (computational domain) for numerical analysis in the 2D model.

2.1. Boundary Conditions

While defining a mesh for CFD simulation, initial boundary conditions are considered to get close to accurate results. Boundary conditions exhibit the characteristics function between the system and the surroundings.

The initial boundary conditions for Temperature (T), Pressure (*p*), Hydrostatic Pressure (P_rgh) and Velocity (*u*) are defined. (See Appendix)

2.2. Initial Assumptions

The flow is laminar and steady-state with Reynolds number (Re) between 200-800.

The collector receives maximum irradiance of the day.

The initial air flowrate is 0.34 m^3/sec or 2.74 m/sec.

The insulating materials has a thermal conductivity (α) of 0.04 J/sec.m.K

The kinematic pressure (p) is constant as that of the atmospheric pressure.

2.3. Mesh Generation

The design is based on the concept of a novel crop dryer. It is slightly modified by creating a small gap called a separating wall in the middle of the dryer chamber to enhance the dryer performance by increasing the airflow rate. The inlet and outlet orifice of the dryer is a rectangular opening on the outside and a sharp triangular notch inside to improve the airflow rate and performance. The 3D solar dryer was developed and meshed in ANSYS Fluent. The structure has a rectangular geometry along the Y-axis and an obstacle (wall) in the middle. The top wall of the solar dryer is inclined at 30^0 while the bottom wall and sides walls are a symmetrical plane. The hot air flow from the inlet at a higher temperature circulates inside the dryer chamber and exits from the outlet at a much lower temperature.

For better results and predictions, the mesh is sliced from the middle to form 2D geometry and post-processing using the inbuilt application *Paraview*.

The dryer measurement and parts are shown in figure:

- Inlet - patch
- Outlet- patch
- Top- Wall
- Bottom- Wall
- Front and Back Walls - Wall
- Left and Right Walls – Wall
- Separating wall – Obstacle

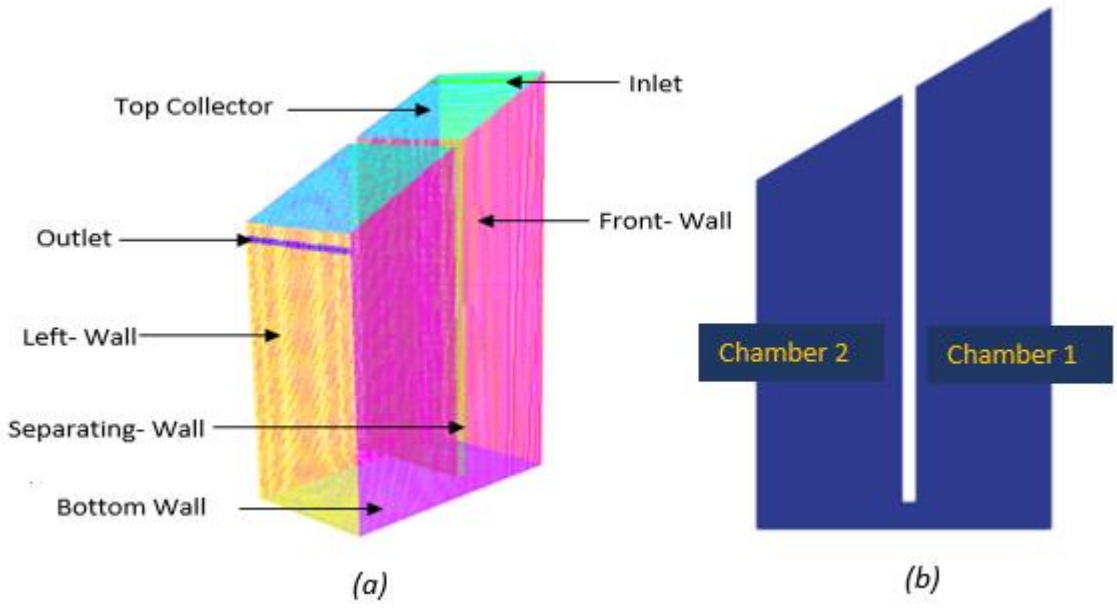

Figure 4.1: Computational flow domain of Novel solar dryer, (a) Mesh view. (b) Slice view.

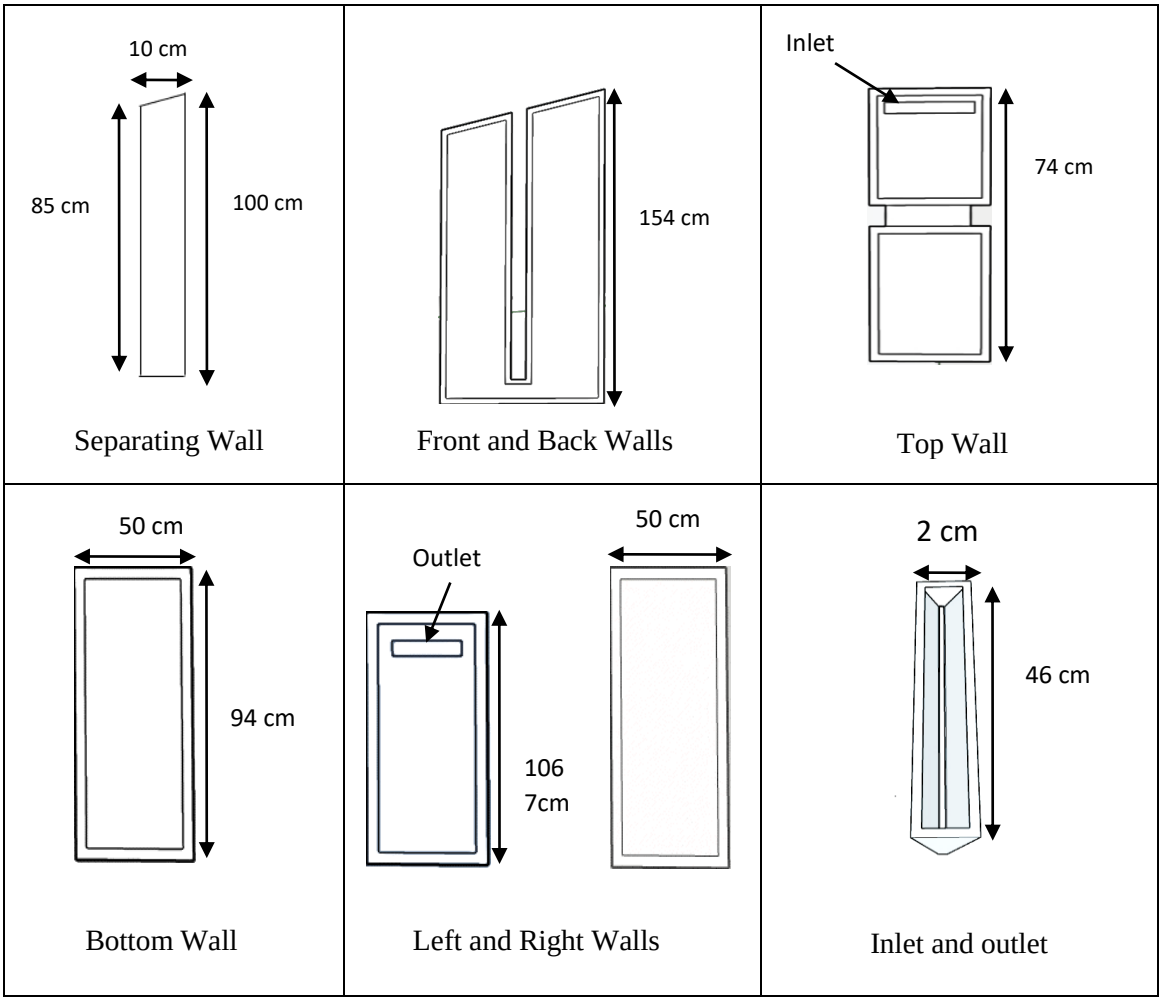

Figure 2.2: Novel Solar dryer measurement and Parts

2.4. Governing Equations for Numerical Solutions

The partial differential equations involving incompressible viscous fluid flow is described by Navier-Stokes equations and are solved using Guess-Seidel method (Fumiya, 2016). The Navier-Stokes equations for buoyancy effect, steady-state laminar flow is solved using solver code *buoyantSimpleFoam* in Openfoam v7 as:

2.4.1. Mass Conservation (Continuity) Equations:

$$\nabla.(\rho u) = 0$$

Where $\rho = desityfield$

$u = velocityfield$

2.4.2. Momentum Equation:

$$\nabla.(\rho uu) = -\nabla p + \rho g + \nabla.\left(2\mu_{eff}D(u)\right) - \nabla\left(\frac{2}{3}\mu_{eff}(\nabla.u)\right)$$

Where p= static pressure field, g = gravitational acceleration.

μ_{eff}= The effective viscosity which is equal to sum of the molecular and turbulent viscosity and the rate of strain tensor, $D(u)$.

2.4.3. Energy Balance Equation

$$\partial(\rho uh) + \nabla.(\rho uK) = \nabla(\alpha.\nabla h) + \rho u.g$$

Where $\alpha = Thermal\ diffusivity\ of\ the\ medium.\ \alpha = \rho\frac{k}{C_p}$, k = Thermal conductivity, $C_p = Specific\ heat\ of\ air\ at\ constant\ pressure.$

K = kinetic energy per unit mass, h = sum of internal energy per unit mass (e) and kinematic pressure $\left(\frac{p}{\rho}\right)$, ($h = e + \frac{p}{\rho}$).

2.5. Heat Transfer Equation (Q)

The heat transfer (Q) is defined as the natural phenomenon of transfer of energy from hot body to cold body in the form of heat for a given system. Thus, it is a measure of kinetic energy possessed by the particles when there is temperature difference between hot and cold body (s). The degree of heat transfer depends on mass (m) of the system, specific heat capacity (c) and the temperature difference (ΔT) between hot and cold body for a given system. Hence, heat transfer equation is given by:

$$Q = mc\Delta T$$

Where Q = Heat transfer

Mode of heat transfer:

i. Heat transfer by Conduction

$$Q = \frac{kA(T_{hot} - T_{cold})t}{d}$$

ii. Heat transfer by Convection

$$Q = hA(T_{hot} - T_{cold})$$

iii. Heat transfer by Radiation

$$Q = \sigma A(T_{hot} - T_{cold})$$

Where, *k = Thermal Conductivity*

A = Surface Area

T_{hot} *= Hot Temperature*

T_{cold} *= Cold Temperature*

t =Time

σ *= Stefan Boltzmann Constant*

h = Heat transfer coefficient

Note: This dissertation discusses only heat transfer by convection.

2.6. Convective heat transfer coefficient (h)

Convective heat transfer coefficient (h) is defined as, the amount of heat transfer per unit temperature difference between the solid surface and the fluid (air in this case) per unit surface area.

Where; h= convective heat transfer coefficient ($W.m^{-2}$ K), q = heat flux density ($W.m^{-2}$)

ΔT = temperature difference (K), m= mass of the sample (air), and c =specific heat capacity.

The h-value varies depending upon the mode of heat transfer. For natural convection heat transfer natural convection, it typically ranges from (2 .5 to 25). The higher the value of h, the higher will be the rate of heat transfer.

The convective heat transfer coefficient (h) in terms of designing a solar dryer is the transfer of heat between the absorber plate and the air passing through the dryer chamber.

Notice that heat transfer coefficient (h) is not a property of fluid but it is dependent on other physical parameters such as surface area, nature of the fluid flow, and velocity of the flow.

2.7. Courant Number (C_o) / Courant-Friedrichs-Lewy Number (CFL number)

The Courant number provides information about the Spatio-temporal discretization of the transport equation. It is the measure of the number of mesh cells that the fluid can travel across in a single time step. For an explicit time-scheme function, the courant number should be less than one (<1) for the solution to successfully converge. Mathematically, C_o is the fluid with a velocity of u across the cell of distance Δx. It is a dimensionless value and hence has no unit.

Mathematically, it can be expressed as,

$$C_o = \frac{u.\Delta t}{\Delta x}$$

Where, C_o = Courant number,

u = Velocity of the airflow

Δx = Length of each cell of the mesh.

2.8. Prandtl number (Pr)

In fluid dynamics, the Prandtl number is the ratio of momentum diffusivity (kinematic viscosity) to thermal diffusivity (0.71 for air at room temperature).

$$Pr = \frac{v}{\propto}$$

Pr = Prandtl number

v = momentum diffusivity

$\propto$= thermal diffusivity

Prandtl number (*Pr*) is significant in the studies of behaviour of the fluid flow as small value of Prandtl number ($Pr << 1$) indicates thermal diffusivity (heat transfer due to conduction only) and Prandtl number ($Pr >> 1$) indicates momentum diffusivity in the system (heat diffuse quicker than velocity).

3. CHAPTER 3: Results and Discussions

3.1. Temperature variation inside the dryer chamber

The table 3.1. shows the minimum time required to reach the maximum average temperature (T_{max} = 82 ^{0}C/355 K) inside the dryer chamber under different heat transfer coefficient (h). The heat transfer coefficient (h) is defined for all sides of the flow domain/dryer. The value of (h) impacts the temperature variations inside the flow domain and therefore, effects the time taken to reach (T_{max}).

Sl. No.	Heat Transfer Coefficient (h)	Time in minute
1	h=0 (zero gradient)	27 mins
2	h=1	32 mins
3	h=2	39 mins
4	h=3	43 mins
5	h=4	49 mins
7	h=5	55 mins

Table 3.1: Time taken to reach Maximum Average Temperature (T_{max}) for different values of Heat Transfer Coefficient (h).

3.1.1. Case I: Zero Gradient Boundary Condition: Adiabatic Wall

The figure 3.1. shows the minimum time required to reach maximum average temperature (T_{max}) in the flow domain. Figure 3.1a. shows the initial conditions before a fixed value of maximum inlet temperature (T_{in}) is injected at the inlet and figure 3.1f shows the minimum time taken to reach close to (T_{max}) after fixed value of (T_{in}) is injected.

From the CFD simulation, the results show that it takes approximately 27 minutes to reach close value of maximum average temperature (i.e., T_{max} = 82 ^{0}C/355 K) inside the dryer chamber. The outlet temperature (T_{out}) was recorded approximately 81.6 ^{0}C at threshold time, t_{th} = 27 minutes as shown in figure 3.1f. The time at which the value of (T_{max}) becomes almost equals to (T_{in}) is called threshold time.

Fig 3.1a: Time, t =0 mins

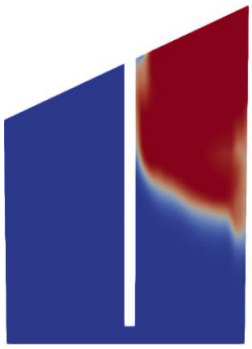

Fig 3.1b: Time, t = 4 mins

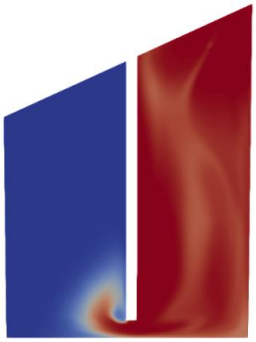

Fig 3.1c: Time, t = 8 mins

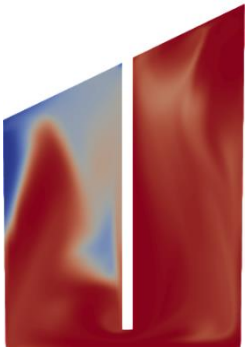

Fig 3.1d: Time, t =12 mins

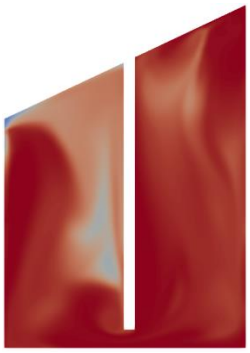

Fig 3.1e: Time, t =16 mins

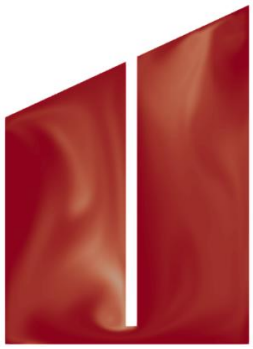

Fig 3.1f: Time, t =27 mins

Figure 3.1: Time taken to reach maximum average temperature in adiabatic wall condition.

The figure 3.2. shows the measure of temperature at different points inside the dryer chamber/domain starting from the bottom (start from 0) to the top of the domain. T_{ch1} and T_{ch2} represents temperature variation in chamber 1 and chamber 2 respectively. The temperature is not constant throughout the domain indicating the non-uniformity of temperature distribution and significant temperature drop at the middle of both Ch1 and Ch2. The temperature drops at the middle as compared to top and bottom of the both the chambers is due to the high concentration of existing air bubbles at room temperature.

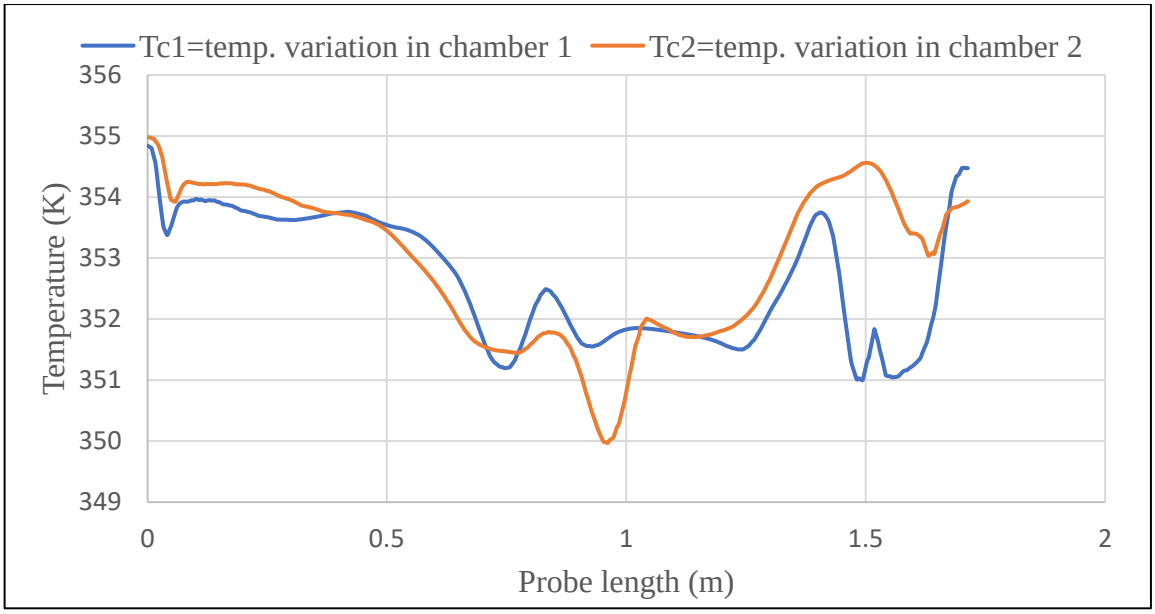

Figure 3.2: Temperature variations in Chamber 1. and Chamber 2. with adiabatic wall.

3.1.2. Case II: External Wall Heat Flux Boundary Condition: Exothermic Walls

The case discusses the amount of time required to reach the maximum average temperature (T_{max}) in the dryer chambers for external wall heat flux boundary condition. In this case, the internal walls of the flow domain are considered as an exothermic boundary by applying heat flux on an internal wall of the dryer cabinet so that certain degrees of temperature are loss to the surroundings.

In reality, there will always be temperature loss to the surrounding. The measure of loss depends on the type of insulation materials being used. The temperature losses from the flow domain can be computed in CFD by introducing thermal conductivity (*k*). For most insulating materials, the k- value ranges from 0.028 W/m.K to 0.15 W/m.K (Table, 3.2). Some of the major factors effecting thermal conductivity (*k*) are temperature, moisture content and humidity (Anh, et. al., 2021). All sides of the domain are considered with good thermal insulation having a thermal conductivity (*k*) of 0.04 W/mK. Generally, a material with higher value of (*k*) indicates poor insulation strength (Özlüsoylu, et. al.,2019).

Type of material	Thermal conductivity coefficient (W/mK)
Wood shavings	0,09-0,15
Wood barks	0,061-0,076
Rock wool	0,04
Glass wool	0,04
Extruded polystyrene foam (XPS)	0,028-0,031
Expanded polystyrene foam (EPS)	0,04
Polyurethane	0,035
Glass foam	0,052
Phenol foam	0,04
Cork boards	0,04-0,055

Table 3.2: Thermal conductivity coefficients of various thermal insulation materials. Özlüsoylu, et. al., (2019).

From the CFD simulation, the results show that it takes 55 minutes to reach the *maximum inlet temperature* (T_{in} = 82 ^{0}C/355 K) inside the dryer chamber which is equivalent to maximum average temperature (T_{max}) from the inlet to the outlet of the domain. The maximum outlet temperature (T_{out}) was recorded at 81.29 ^{0}C at time t = 55.26 minutes which is also a threshold time (t_{th}) as shown in sub-figure 3.3f. After reaching (T_{max}), there is no significant rise in the domain temperature with respect to time. Hence, the increase in temperature is linear with respect to time (t) till it reaches to (T_{max}).

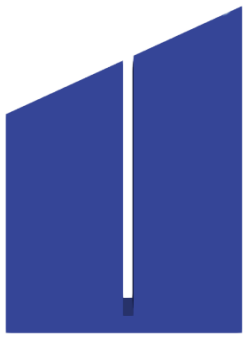

Fig. 3.3a: Time, t = 0 mins

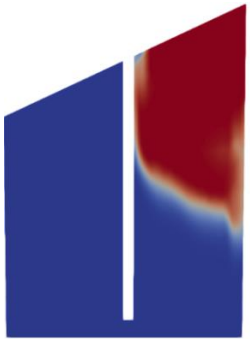

Fig.3. 3b: Time, t = 5 mins

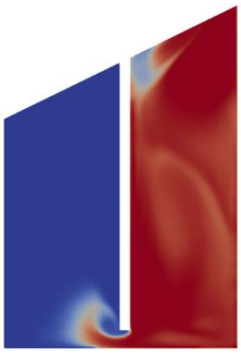

Fig. 3.3c: Time, t = 12 mins

Fig.3.3d: Time, t = 20 mins *Fig. 3.3e: Time, t = 30 mins* *Fig.3.3f: Time, t = 55 mins*

Figure 3.3: Time taken to reach maximum average temperature in exothermic wall condition.

The figure 3.4. shows the measure of temperature at different points inside the dryer chamber/domain starting from the bottom (start from 0) to the top of the domain. T_{c1} and T_{c2} represents temperature variation in chamber 1 and chamber 2 respectively. The temperature is not constant throughout the domain and hence, it indicates that there is non-uniformity of heat distribution. Further, there is a significant temperature drop at the bottom and top of Ch2. Similarly, there is a significant temperature drop at the top in Ch1. However, the temperature drops are at different locations as compared from case I., due to introduction of heat flux in case II.

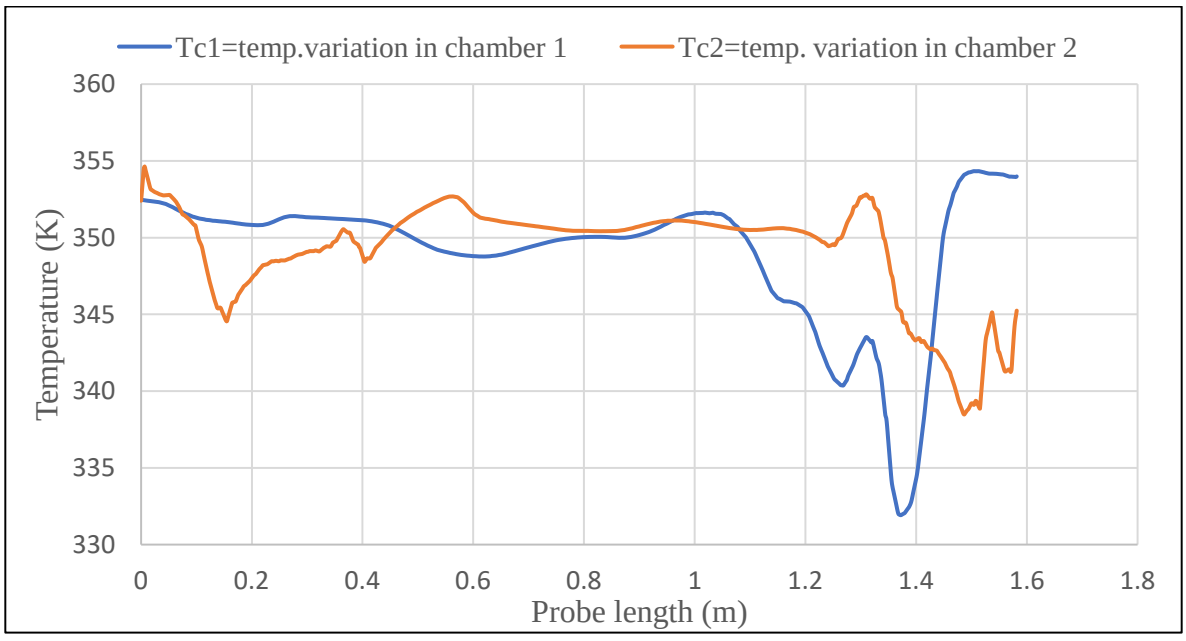

Figure 3.4: Temperature variation in Chamber 1. and Chamber 2. with exothermic wall.

For comparison study, the temperature inside the solar dryer over timestep (s) is plotted for different heat transfer coefficient (h) for internal walls of the dryer. The figure 3.5, represents the temperature variations inside the flow domain for a fixed inlet velocity (u) of 2.74 m/sec and (T_{in}) of 82 ^{0}C/355 K. $T_{avg}.(h0)$ represents the average temperature variation for h=0 or adiabatic wall. Similarly, $,T_{avg}.(h2)$, $T_{avg}.(h3)$ and $T_{avg}.(h5)$ represents average temperature variation for values of h=2, h=3 and h=5 respectively. The simulation is run for 25 minutes and plotted the graph between temperature vs time along y-axis direction. From figure 3.5, it indicates the time required to reach the maximum average temperature (T_{max}) in the dryer takes longer duration for higher values of heat transfer coefficient (h).

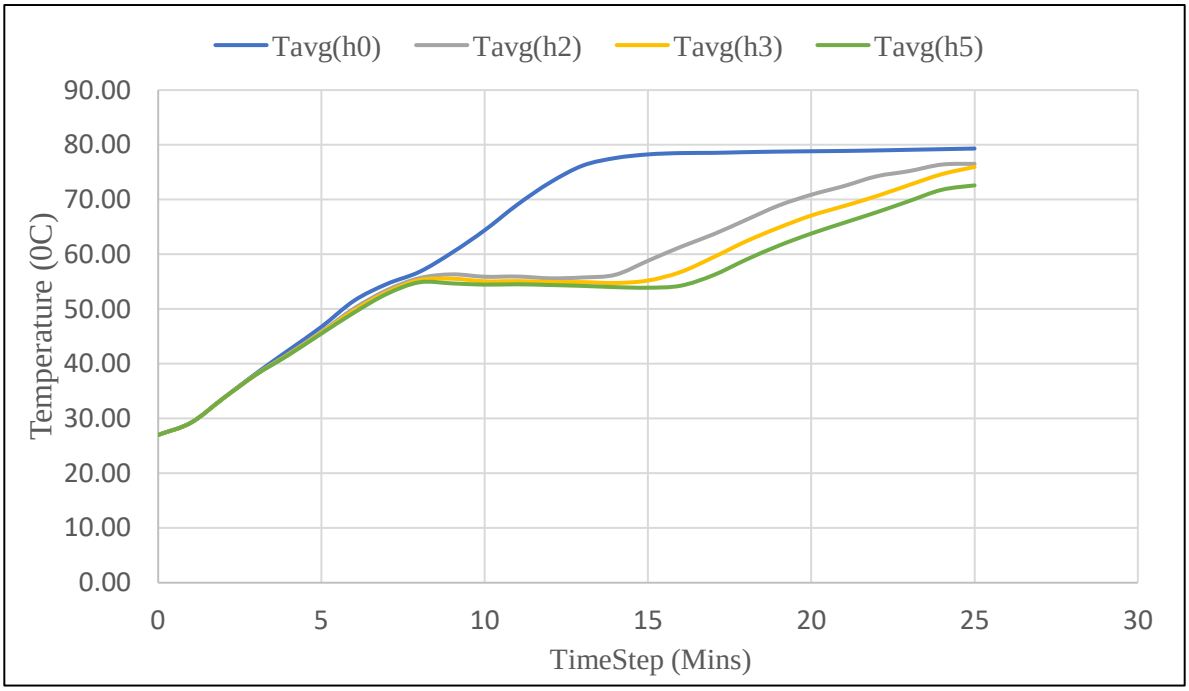

Figure 3.5: Impact of heat transfer coefficient (h) on maximum average temperature inside the solar dryer w.r.t, time.

3.2. Air flowrate (U)

The figure 3.6. shows the average flowrate at outlet of the solar dryer for different heat transfer coefficient (h). The flowrate at the inlet is constant with respect to time and is independent of h-value. However, the flowrate decreases with time with higher values of heat transfer coefficients.

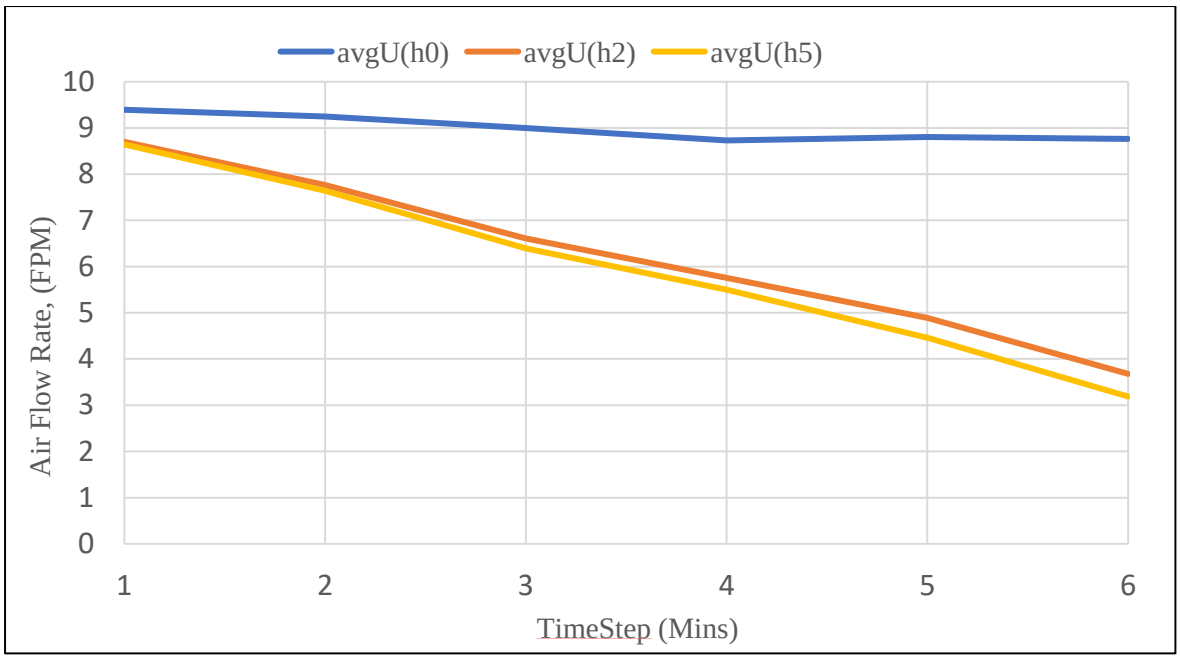

Figure 3.6: Comparison of air flowrate (U) for different heat transfer coefficients (h).

The air flowrate is found to be highest for h= 0 at U = 8,765 feet/min and lowest for h=5 at U = 3.187 feet/min in Chamber 1. When the temperature inside the dryer chamber reaches to its threshold temperature (T_{th}) in chamber 2, the maximum average flowrate at the outlet is found to be 10.056 feet/min and 7.837 feet/min. for h=0 and h=5 respectively. The flowrate at the inlet is constant irrespective of the heat transfer coefficient (h), (appendix, Table 7.2).

3.3. Heat Transfer (Q)

In this study, the heat transfer (Q) is computed from the inlet to the outlet of the designed natural convection Novel solar Dryer for 25 minutes. Qh_2, Qh_3, Qh_4 and Qh_5 are the heat transfer for different values of heat transfer coefficient(h) in exothermic wall conditions and Qh_0 is for adiabatic wall condition as shown in figure 3.7.

The x-axis represents the heat transfer (Q) from inlet to outlet of the medium and Y-axis represents the Time (t) in minutes. The heat transfer was calculated using the equation, Q= mc(ΔT); where, m = the mass of the medium (i.e., Solar dryer, 32 kg) in kg, c = specific heat capacity of the air at constant pressure and room temperature (c = 1.005 kJ/kg.^{0}C) and ΔT = temperature difference in ^{0}C between outlet and inlet of the solar dryer (T_{out}-T_{in}).

The comparison study shows that the heat is quickly transferred with lower values of heat transfer coefficient (h) and vice-versa.

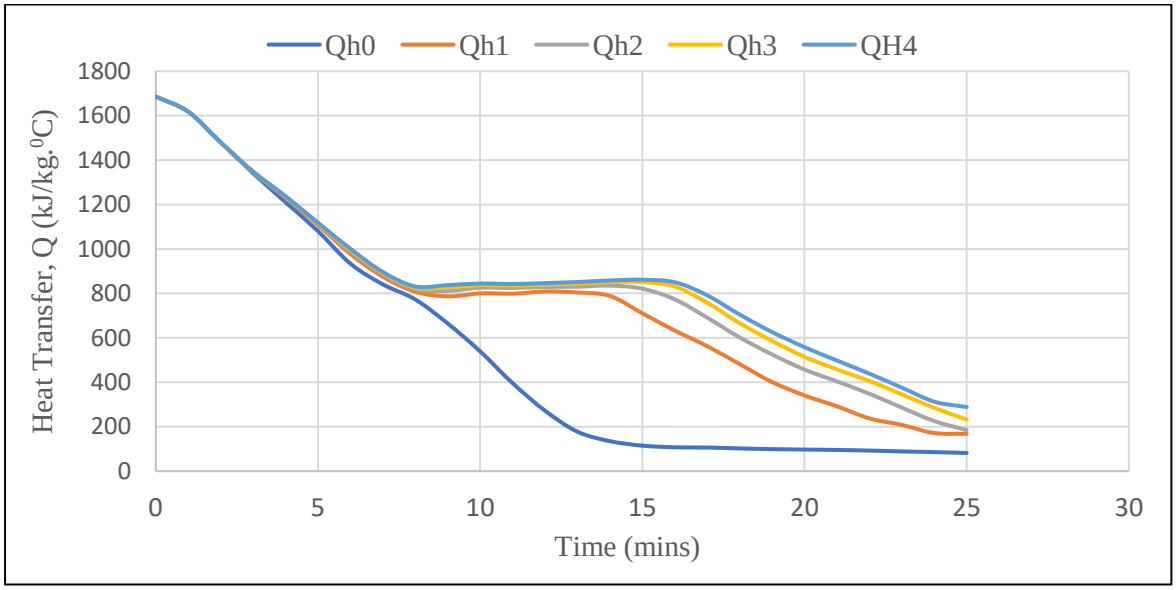

Figure 3.7: Heat transfer (Q) from inlet to outlet of the designed solar dryer w.r.t time.

The heat transfer is maximum at the beginning and becomes minimum when the temperature inside the dryer reaches to threshold temperature (t_{th}). Table 3.3, shows the different values of heat transfer coefficient (h) and amount of heat transferred from the inlet to the outlet of the dryer at certain interval of time. The heat transferred is maximum at time, t = 25 mins for h = 0 and minimum at time t= 5 mins for h= 4.

SL.No	Qh0 (kJ/kg.^{0}C)	Qh1 (kJ/kg.^{0}C)	Qh2 (kJ/kg.^{0}C)	Qh3 (kJ/kg.^{0}C)	Qh4 (kJ/kg.^{0}C)	Amount of heat transferred in *x* time
1	1603.585538	1517.575	1500.532	1453.235	1396.988	25 mins
2	1588.28994	1344.786	1228.399	1171.079	1127.368	20 mins
3	1570.664753	975.148	864.2779	834.6676	824.1538	15 mins
4	1146.342195	885.3975	860.1092	848.4305	841.2885	10 mins
5	605.1723075	577.8916	572.9259	569.6767	567.3471	5 mins

Table 3.3: Amount of heat transferred from inlet to outlet of the designed solar dryer in certain period of time.

3.4. Velocity Distribution (u)

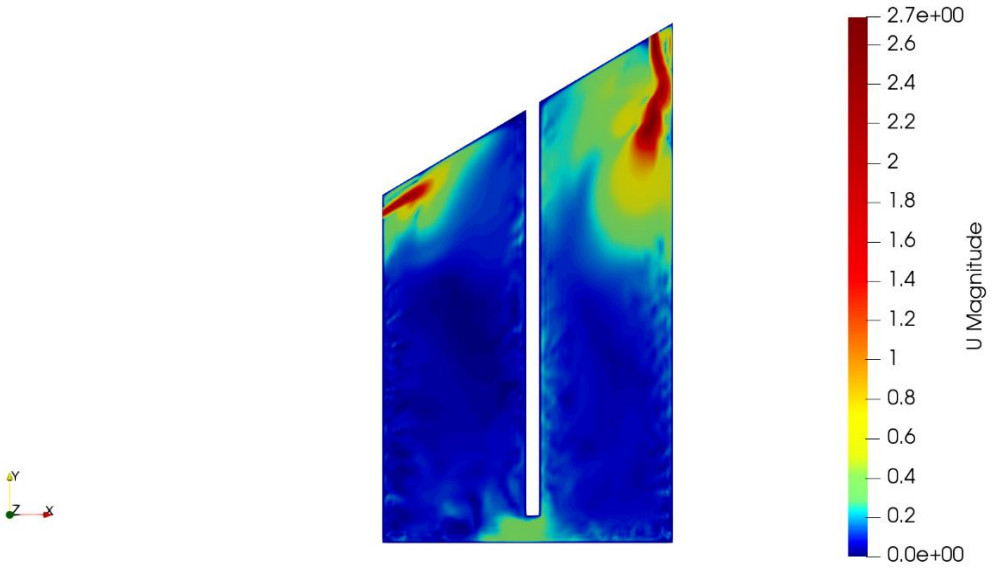

Figure 3.8: Velocity (u) distribution inside Dryer Chamber 1. and Chamber 2.

This non-uniform distribution of airflow inside the dryer chamber is studied. Firstly, the dryer is divided into two parts (chamber 1. and chamber 2). The set of probes is located diagonally along with each chamber and velocity of the air flow is plotted over these points of probes as shown in figure 3.9. Note that the simulation is done for 2D geometry, hence the initial inlet velocity, u = 2.74 m/sec.

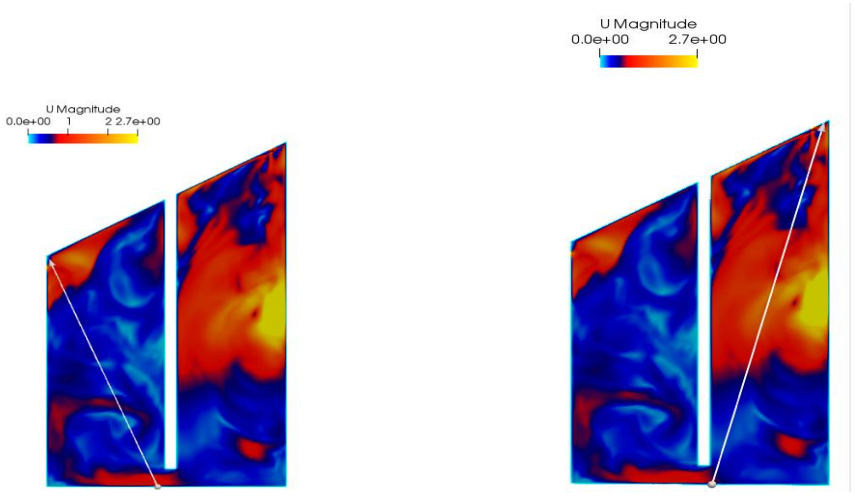

Figure 3.9: Illustration of velocity (u) distribution using Needle Probe

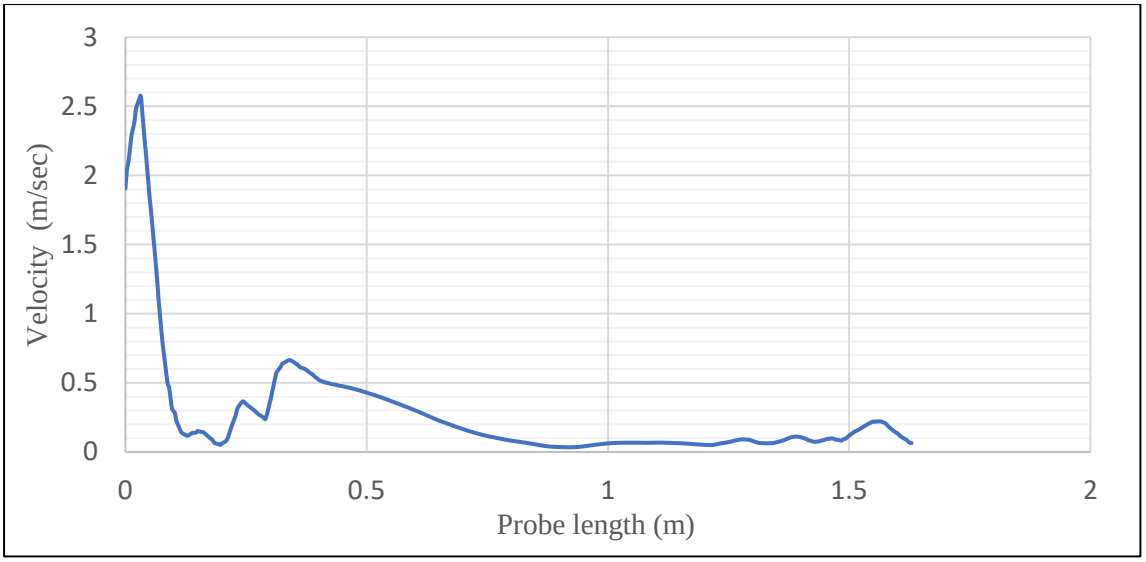

Figure 3.10.1: Velocity (u) distribution in Chamber 1. along Y-axis direction.

Figure 3.10.1. represents the Velocity (u) distribution in Chamber 1. along Y-axis direction. It was observed that the airflow velocity rate is greater at the top and middle with u-value ranging from 1.4 m/sec to 1.85 m/sec. The airflow velocity rate is much lower at the bottom with a u-value as low as 0.2 m/sec.

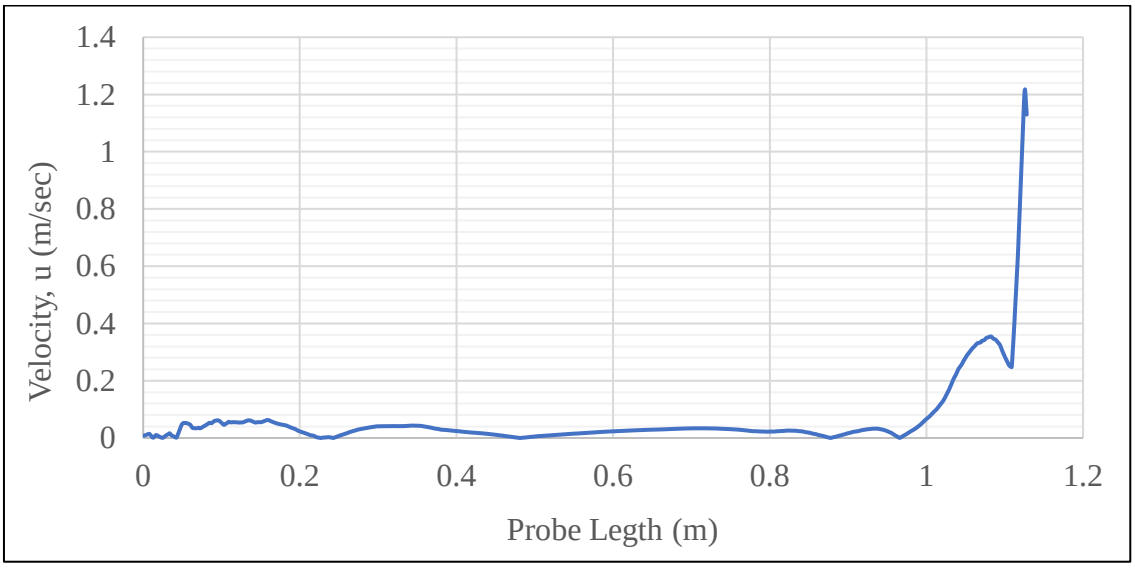

Figure 3.10.2: Velocity (u) distribution in Chamber 2. along Y-axis direction.

Figure 3.10.2. represents the Velocity (u) distribution in Chamber 2. along Y-axis direction. In this case, unlike airflow velocity distribution in chamber 1, it was observed higher at the

bottom of the chamber. The airflow velocity (u) ranges from 0.05 m/sec to 1.05 m/sec. Subsequently, the air velocity in chamber 2. is also low as compared to chamber 1.

4. Further Development

The project is a part of *solar-Food* project and no way proofs the finalised results from the simulation results. Further works can be done to optimised the performance parameters of the proposed solar crop dryer. Here are some of the few things that can be done:

i. The performance of the solar crop and dryer can be improved by incorporating additional heat storage such use of Phase Change Materials (PCM) and heat exchanger.

ii. The simulation results in this report is laminar and steady-state. There is still a room for testing for turbulent and transient-state for further verification.

iii. Comparison analysis of the thermal performance of Novel solar dryer can be iterated with other types of solar dryers through computational studies as well as from experimental.

5. Conclusion

This report highlights the CFD simulation of natural convection Novel solar dryer in the computational domain. The Navier-Stokes partial differential equations governing the incompressible steady-state fluid flow is solved in OpenFOAM solver code *buoyantSimpleFoam* to study the mass, momentum, and energy conservation equation. The results from the CFD simulation is use to evaluate the performance analysis of the dryer. The simulation results proved that the performance of the solar dryer is affected by heat transfer coefficient (h), air flow velocity (*u*) and temperature (T). For optimum performance, the h-value and thermal conductivity must be maintained minimum. The distribution of velocity (u) air flowrate (U) inside the domain (chamber 1. and chamber 2.) is not uniform and therefore, there is variation in temperature. The heat transfer is maximum at the middle of both the chambers and diffuses at the bottom and corners of the chamber in case 1. The heat transfer is maximum at the bottom and top of the chambers in case 2. The heat transfer with respect to flowrate is also seen faster in chamber 1 as compared to chamber 2. Hence, addition of forced heat convective device such as fans at chamber 2. can greatly enhance performance of the dryer with short drying time.

6. Bibliography

Adelaja.O, Babatope, B.I., (2013). Analysis and Testing of a Natural Convection Solar Dryer for the Tropics. Journal of Energy. Article ID 479894, pp:8.

Anand Chavan, Vivek Vitankar, Nikhil Shinde & Bhaskar Thorat (2021). CFD simulation of solar grain dryer, Drying Technology,

Anh, H. D. L., Pásztory, Z., (2021). An overview of factors influencing thermal conductivity of building insulation materials. Journal of Building Engineering, Vol: 44, ISSN 2352-7102, https://doi.org/10.1016/j.jobe.2021.102604.

Demissie, P., Hayelom, M., Kassaye, A., Hailesilassie. A., Gebrehiwot, M., & Vanierschot, M., (2019). Design, development and CFD modelling of indirect solar food dryer, Innovative Solutions for Energy Transitions. Pg: 1128-1134, issn:1876-6102, vol:158, Energy Procedia.

Benjamin, D., (2017). Performance Evaluation of a mixed-mode solar dryer incorporating a backup heater for drying Cocoyam, Dissertation Paper, Kwame Nkrumah University of Science and Technology, College of Engineering, Department of Agricultural and Biosystem Engineering.

Fumiya, (2016). CFD with a Mission, https://caefn.com/openfoam/solvers-buoyantpimplefoam.

Ghatrehsamani S.H., Dadashzadeh M. and Zomorodian A. (2012). Kinetics of Apricot Thin Layer Drying in a Mixed and Indirect Mode Solar Dryer, International Journal of Agriculture Sciences, ISSN: 0975-3710 and E-ISSN: 0975-9107, pp:4-6.

Gupta, S.K. & Sootha, G.D., (1982). Performance Study of Solar Dryer. Book of Passive and Low Energy Alternatives, the first International PLEA Conference, Bermuda. https://www.sciencedirect.com/book/9780080294056/passive-and-low-energy-alternatives-i.

Hoffmann, H., Matavel, E. C., Rybak., C., Hafner, J.M., et. al., (2021). Experimental evaluation of a passive indirect solar dryer for agricultural products in Central Mozambique, Journal of Food Processing and Preservation, DOI: 10.1111/jfpp.15975, pp: 1-2.

Senate, I.N., (2003). Optimization of mixed-mode and indirect-mode natural convection solar dryers. Renewable Energy 28: 435-453.

Ismail, R.M., (2019). Design a solar dryer with integrated thermal storage based on sorption materials. Dissertation Institute for water and energy sciences, PAN-AFRICAN University, Algeria.

Ministry of Agriculture and Forests, (2015), Annual Statics report, 2015. Department of Agriculture, Thimphu: Bhutan.

Ministry of Agriculture and Forests (2021). SELF-SUFFICIENCY AND DIETARY ENERGY SUPPLY OF FOOD CROPS IN BHUTAN (A STATUS REPORT) OCTOBER 2021.), Department of Agriculture. Thimphu: Bhutan, ISBN 978-99936-957-9-0.

Ministry of Agriculture and Forests, (2021). Agriculture Research and Development Highlights 2018-2019, Department of Agriculture. Thimphu: Bhutan.

Nortan, B., (2022). Solar Dryer Types. Industrial and Agricultural Applications of Solar, Heat,Comprehensive Renewable Energy, 2nd ed; Vol:9, pp: 638-669. ISBN 9780128197349, https://doi.org/10.1016/B978-0-12-819727-1.00076-5.

Nwakuba, N., Ndukwe, S. & Paul, T., (2020). Influence of product geometry and process variables on drying energy demand of vegetables: An experimental study. Journal of Food Process Engineering, Owerri, Nigeria, pp:4-6.

Olaoye, O.S, Waheed, M.A, & Lucas, E.B., (2014). Experimental Studies of Effects of Geometry on Drying Rate and Properties of Ginger (Zingiber officinale Rosc.) with Solar-hybrid Dryer. Journal of Biology, Agriculture and Healthcare, Ogbomoso, Nigeria. www.iiste.org ISSN 2224-3208 (Paper) ISSN :2225-093X (Online) Vol.4, No.24, pp: 46-47.

Özlüsoylu, I, & İstek, A., (2019), The Effect of Hybrid Resin Usage on Thermal Conductivity in Ecological Insulation Panel Production, 4th International Conference on Engineering Technology and Applied Sciences (ICETAS), Kiev, Ukraine. Pp- 293-294.

Probert, A., (2022). Development and Testing of Novel Solar Dryer Design with an incorporated Heat Exchanger, for use in the Himalayan Regions. Division of Heat Transfer, Department of Energy Sciences, Faculty of Engineering, Lund University, Sweden. ISSN: 0282-1990, pp: 1-2, 15-24.

Sanghi, et. al., (2017). CFD simulation of corn drying in a natural convection solar dryer. Crop Drying Technology. https://doi.org/ 36.10.1080/07373937.2017.1359622, pp: 2-6

Tamate, M., Virupakshar, A., Satish, J., & Madhusudhana, K., (2017). Design and Development of Solar Multi-Crop Dryer. International Journal of Darshan Institute on Engineering Research & Emerging Technology, Karnataka, India. Vol:6, No.2, p: 11.

Versteeg, H.K., & Malalasekera, W., (2007). An Introduction to Computational Fluid Dynamics, Pearson Education Limited, Edinburgh Gate, Harlow Essex CM20 2JE, England. ISBN: 978-0-13-127498-3, Ed: 2nd, pp: 1-2.

Wangmo, Changa & Dendup, Tashi. (2021). Post-Harvest Handling and Losses of Green Chilies: A Case Study from Bhutan. Indonesian Journal of Social and Environmental Issues, pp: 16-27.

Design, Construction and Performance Evaluation of Mixed-Mode Solar Drying System for Crops, Department of Materials Sciences and Engineering, African University of Science and Technology. P.M.B 681, Garki, Abuja F.C.T, Nigeria.

Weller, H. G., Tabor, G., Jasak, H. & Fureby, C., (1998). A tensorial approach to computational continuum mechanics using object-oriented techniques, COMPUTERS IN PHYSICS, VOL. 12, NO. 6, NOV/DEC. http://dx.doi.org/10.1063/1.168744.

7. Appendix

7.1. Average temperature for different h-values in ^{0}C.

	h=1 J/kg	h=2 J/kg	h=3 J/kg	h=4 J/kg	h=5 J/kg
TimeStep (s) (mins)	Tmax (^{0}C)	Tmax (^{0}C)	Tmax (^{0}C)	Tmax (^{0}C)	Tmax (^{0}C)
0.0	27.01	27.01	27.01	27.01	27.01
1.0	29.23	29.22	29.22	29.22	29.22
2.0	33.74	33.72	33.72	33.72	33.72
3.0	38.25	38.08	38.04	38.03	38.02
4.0	42.51	41.85	41.72	41.67	41.63
5.0	46.75	45.86	45.70	45.59	45.52
6.0	51.53	50.10	49.75	49.51	49.35
7.0	54.57	53.44	53.09	52.89	52.75
8.0	56.79	55.65	55.29	55.06	54.89
9.0	60.31	56.33	55.54	55.04	54.69
10.0	64.41	55.89	55.07	54.69	54.45
11.0	69.08	55.94	55.10	54.74	54.52
12.0	73.12	55.62	54.95	54.61	54.39
13.0	76.20	55.76	54.92	54.48	54.23
14.0	77.59	56.26	54.75	54.24	54.00
15.0	78.25	58.82	55.20	54.24	53.90
16.0	78.49	61.35	56.77	54.89	54.26
17.0	78.53	63.65	59.45	57.26	56.18
18.0	78.66	66.28	62.36	60.28	59.00
19.0	78.76	68.91	64.86	62.87	61.57
20.0	78.82	70.88	67.08	65.21	63.79
21.0	78.88	72.47	68.82	67.05	65.75
22.0	78.98	74.25	70.63	68.76	67.68
23.0	79.09	75.20	72.67	70.72	69.73
24.0	79.20	76.40	74.64	72.70	71.79
25.0	79.32	76.52	75.96	74.42	72.58

Table 7.1. Average temperature for different h-values in ^{0}C.

7.2. Average flowrate (U) in Feet/minute.

Time (mins)	avgU(h0) (Feet/min)	avgU(h2) (Feet/min)	avgU(h3) (Feet/min)	avgU(h5) (Feet/min)
0	0	0	0	0
1	9.39346892	8.69941611	8.66509644	8.64282705
2	9.24488818	7.76402297	7.68924035	7.64103923
3	8.99691232	6.6048136	6.47462332	6.39302796
4	8.72964026	5.7591281	5.6075151	5.49923979
5	8.80668723	4.8933588	4.64548139	4.45970624
6	8.76547606	3.67846611	3.36655682	3.18771255
7	8.88538816	2.32869692	2.01816593	1.82492827
8	8.61441438	1.313689234	1.052083956	0.927895188
9	8.95568146	0.601102227	0.578797395	0.610421504
10	8.90417242	0.624041077	0.808270562	0.939234659
11	9.56615022	1.83947918	2.09527197	2.19387949
12	8.84289714	2.20187363	2.43267981	2.53394548
13	8.91557293	2.72708469	3.01258969	3.11631661
14	10.00872235	3.22213067	3.56268891	3.67338609
15	9.94707296	3.64552474	3.86648592	3.91640007
16	10.1307019	3.82198652	4.02585678	4.12863858
17	10.08762018	4.2756835	4.2928138	4.32532199
18	10.0761606	4.85766083	4.83037049	4.78004285
19	9.96489241	5.51621257	5.52054437	5.38637671
20	10.08874251	6.06509101	6.15913045	6.00923048
21	10.04971693	6.45680387	6.67504783	6.47657263
22	10.08498172	6.75093309	7.05313521	6.84997379
23	10.06582335	6.99396676	7.37591338	7.18052951
24	10.11955736	7.19498197	7.66232412	7.48066418
25	10.05654936	7.40217984	7.96143491	7.83776202

Table 7.2: Average flowrate (U) in Feet/minute for different h-values of the internal Walls

7.2. Zero Gradient Initial Boundary Condition

7.2.1. Kinematic Pressure (p)

```
boundaryField
{
  wall-part_2-solid
    {
      type                    zeroGradient;
    }
    inlet
    {
       type                   zeroGradient;
    }
    outlet
    {
      type                    fixedValue;
      value                   uniform 100000;
    }
    leftandright
    {
        type                  zeroGradient;

    }
    frontandback
    {
        type                  zeroGradient;
    }
    top
    {
        type                  zeroGradient;
    }
    bottom
    {
       type                   zeroGradient;
    }
    separationwall
    {
      type                    zeroGradient;
    }
```

7.2.2. Hydrostatic Pressure (p_rgh)

```
boundaryField
{
    wall-part_2-solid
    {
       type                zeroGradient;
    }
    inlet
    {
       type                fixedValue;
       value               $internalField;
    }
    outlet
    {
        type               fixedValue;
       value               $internalField;
    }
    leftandright
    {
      type                 zeroGradient;
    }
    frontandback
    {
       type                zeroGradient;
    }
    top
    {
       type                zeroGradient;

    }
    bottom
    {
       type                zeroGradient;
    }
    separationwall
    {
       type                zeroGradient;
    }
```

7.2.3. Temperature (T)

```
boundaryField
{
     wall-part_2-solid
    {
         type                zeroGradient;

    }
    inlet
    {
        type                 fixedValue;
        value                uniform 355;
    }
    outlet
    {
     type                    zeroGradient;

    }
    leftandright
    {
      type                   zeroGradient;
    }
    frontandback
    {
       type                 zeroGradient;
    }
    top
    {
       type                 zeroGradient;
    }
    bottom
    {
    type                    zeroGradient;
    }
    separationwall
    {
       type                 zeroGradient;
    }
```

7.2.4. Velocity (u)

```
boundaryField
{
     wall-part_2-solid
    {
         type               noSlip;
    }
    inlet
    {
       type                 fixedValue;
       value                uniform (0 -2.74 0);

    }
    outlet
    {
       type                 zeroGradient;

    }
    leftandright
    {
      type                  noSlip;
    }
    frontandback
    {
       type                 noSlip;
    }
    top
    {
        type                noSlip;
    }
    bottom
    {
        type                noSlip;
    }
    separationwall
    {
        type                noSlip;
    }
```

7.3. External wall heat flux temperature: Boundary field for (p), (p_rgh) and (u) remain same except Temperature (T) as shown below.

```
boundaryField
{
     wall-part_2-solid
    {
         type               externalWallHeatFluxTemperature;
         mode               coefficient;
         thicknessLayers    (0.05);
         kappaLayers        (0.04);
         Ta                 uniform 300;
         kappaMethod        fluidThermo;
         h                  uniform 5;
         value              $internalField;;

    }
    inlet
    {
        type                fixedValue;
        value               uniform 355;
    }
    outlet
    {
     type                   zeroGradient;

    }
    leftandright
    {
         type               externalWallHeatFluxTemperature;
         mode               coefficient;
         thicknessLayers    (0.05);
         kappaLayers        (0.04);
         Ta                 uniform 300;
         kappaMethod        fluidThermo;
         h                  uniform 5;
         value              $internalField;
    }
```

Continue…

```
}
frontandback
{
   type                zeroGradient;
}
top
{
     type               externalWallHeatFluxTemperature;
     mode               coefficient;
     thicknessLayers    (0.05);
     kappaLayers        (0.04);
     Ta                 uniform 300;
     kappaMethod        fluidThermo;
     h                  uniform 5;
     value              $internalField;;
}
bottom
{
     type               externalWallHeatFluxTemperature;
     mode               coefficient;
     thicknessLayers    (0.05);
     kappaLayers        (0.04);
     Ta                 uniform 300;
     kappaMethod        fluidThermo;
     h                  uniform 5;
     value              $internalField;
 }
separationwall
{
     type               externalWallHeatFluxTemperature;
     mode               coefficient;
     thicknessLayers    (0.05);
     kappaLayers        (0.04);
     Ta                 uniform 300;
     kappaMethod        fluidThermo;
     h                  uniform 5;
     value              $internalField; ;
}
```

End